ICASSP 2023 - 2023 IEEE International Conference on Acoustics, Speech and Signal Processing (ICASSP) | 978-1-7281-6327-7/23/$31.00 ©2023 IEEE | DOI: 10.1109/ICASSP49357.2023.10095766

# RADIO SENSING WITH LARGE INTELLIGENT SURFACE FOR 6G

*Cristian J. Vaca-Rubio*[*,1], *Pablo Ramirez-Espinosa*[2], *Kimmo Kansanen*[3],
Zheng-Hua Tan[1], Elisabeth de Carvalho[1]

[1]Department of Electronic Systems, Aalborg University, Aalborg, Denmark.
[2]Departament of Signal Theory, Telematics and Communications, University of Granada, Granada, Spain
[3]Norwegian University of Science and Technology, Trondheim, Norway
{cjvr*, zt, edc}@es.aau.dk, pre@ugr.es, kimmo.kansanen@ntnu.no

**ABSTRACT**

This paper leverages the potential of Large Intelligent Surfaces (LIS) for radio sensing in 6G wireless networks. By taking advantage of arbitrary communication signals occurring in the scenario, we apply direct processing to the output signal from the LIS to obtain a radio map that describes the physical presence of passive devices (scatterers, humans) which act as virtual sources due to the communication signal reflections. We then assess the usage of machine learning and computer vision methods including clustering, template matching and component labeling to extract meaningful information from these radio maps. As an exemplary use case, we evaluate this method for passive multi-human detection in an indoor setting. The results show that the presented method has high application potential as we are able to detect around 98% of humans passively even in quite unfavorable Signal-to-Noise Ratio (SNR) conditions.

## 1. INTRODUCTION

Sensing can be regarded as the ability of wireless systems to process the signals with the aim of describing the physical environment. There are different methodologies to perform sensing using wireless signals. Essentially, some of these methods use dedicated signals and/or specific hardware [2–9], while others use communication signals of commodity devices to perform the sensing task [10–16]. As an example of the first type, in [4–7] they employ Radio Tomographic Image (RTI), which is a Received Signal Strength (RSS)-based technology for rendering physical objects in wireless networks. They create a radio map based on the RSS variations due to objects presence in the scenario by deploying nodes around the room conforming a Wireless Sensor Network (WSN). In turn, by making use of the communication signals occurring in an environment and avoiding dedicated transmissions [10, 11], one can rely on properties of the wireless channel such as the Channel State Information (CSI) using commodity Wi-Fi devices, to perform sensing tasks as human gesture recognition or fall detection. Works like the ones presented in [2,3,8,9] capture the reflections of wireless signals, similar to the radar principle.

In the context of communications, the Multiple-input Multiple-output (MIMO) technique is a fundamental technology in 5th generation of wireless networks (5G) with the main purpose of increasing area spectral efficiency [17, 18]. Intending to push their benefits to the limit and look towards post-5G, researchers are defining a new generation of base stations that are equipped with an even larger number of antennas. The concept of Large Intelligent Surface (LIS) gained a lot of attraction. It designates a large continuous electromagnetic surface able to transmit and receive radio waves. While the potential for communications of LIS is being investigated, these devices offer possibilities that are not being understudied accurately, i.e., environmental sensing based on radio images [19].

Due to the increasing interest in both sensing and LIS, and motivated by their future integration in communication systems, in this work, we are focusing on LIS sensing capabilities. We make use of a method that enables reconstructing a radio map of the propagation environment using an indoor LIS deployment in the ceiling [1, 20, 21]. This radio map shows the presence of active and passive (scatterers/humans) users in the environment by piggybacking the communication signals. We solve a problem of passive multi-human detection in the scenario using the reconstructed radio maps. Detecting passive humans is of great interest as we are relying on environmental radio signals and do not need dedicated devices. This could be quite to optimize beamforming towards the passive human enabling the access phase with an optimized radiation pattern, for Electromagnetic (EM) avoidance and Physical Layer Security (PLS), where the detection of the passive target is mandatory to perform beamforming. The solution is based on the k-means clustering of the radio maps, followed by the application of image processing to enhance the quality and computer vision to perform the detection. We measure the detection accuracy as the number of users detected while also verifying the positioning accuracy.

## 2. PROBLEM FORMULATION AND SYSTEM DESCRIPTION

Let us consider an indoor scenario where $U$ users are randomly deployed in a room. Within the $U$ users, a subset $U_a$ are commodity wireless devices fulfilling their communication tasks, while $U_p = U - U_a$ users are just passive human beings. The objective is, hence, sensing the position of both the $U_a$ active and the $U_p$ passive humans from the signals radiated by the former. For the sake of simplicity, we assume the $U_a$ users transmit at the same frequency — representing, e.g., Wi-Fi signaling or transmissions at some cellular frequency band. To perform the sensing, we assume that an LIS of $M$ antenna elements is placed along the ceiling, whose physical aperture comprises its whole area. The sensing problem reduces to determine, from the superposition of the received signals from each of the $U_a$ users at every of the $M$ LIS elements, the $(x, y)$

*Corresponding author. This work is the conference version of [1]. This project has received funding from the European Union's Horizon 2020 research and innovation programme under the Marie Skłodowska-Curie Grant agreement No. 813999.

coordinates of the $U_p$ passive humans. The superposed complex baseband signal received at the LIS is given by

$$\mathbf{y} = \sum_{u=1}^{U_a} \mathbf{h_u} x_u + \mathbf{n}, \quad (1)$$

with $x_u$ the transmitted (sensing) symbol from user $u$, $\mathbf{h_u} \in \mathbb{C}^{M \times 1}$ the channel vector from a specific position of user $u$ to each antenna-element, and $\mathbf{n} \sim \mathcal{CN}_M(\mathbf{0}, \sigma^2 \mathbf{I}_M)$ the noise vector. Please note we are considering a narrowband transmission, avoiding frequency selectivity effects.

## 3. LIS RADIO MAP GENERATION

Due to the large physical aperture of the deployment in comparison with the distance between the transmitters and the LIS, spherical wave propagation needs to be taken into account, and thus the channel coefficient $h_{s,i}$ at the LIS $i$-th element from an arbitrary user transmission is proportional to [22]

$$h_{s,i} \propto \frac{1}{d_i} e^{-j \frac{2\pi}{\lambda} d_i}, \quad (2)$$

where $d_i = \sqrt{(x_i - x_u)^2 + (y_i - y_u)^2 + (z_i - z_u)^2}$ denotes the distance between the active device $u$ and the $i$-th antenna, and $\lambda$ is the wavelength. We are interested in determining the spherical steering vector by using (2). For that we define an array of $N \times N$ m aperture with an antenna spacing of $\Delta s = \frac{\lambda}{2}$ resulting in $N_f = \frac{N}{\Delta s} \times \frac{N}{\Delta s}$ antennas and we set a $f$. We then emulate a transmitter in the center position of the filter $(x_u, y_u, z_u) = (\frac{N}{2}, \frac{N}{2}, 6.2)$ m[1]. Next, we compute eq (2) with respect to all the antenna elements from the designed array, obtaining $\mathbf{h_s}$. Figure 1 shows the expected spherical pattern $\mathbf{h_s}$. We are not interested in the absolute phase values but in their variation along the space. In this way, describing the surface in a vectorized notation, we can derive a Matched Filter (MF) such that:

$$\mathbf{y_f} = \mathbf{h_s} * \mathbf{y}, \quad (3)$$

where $*$ denotes the convolution operator. This convolution is performed along all the LIS dimension. Then, $\mathbf{h_s} \in \mathbb{C}^{N_f \times 1}$ denotes the expected spherical pattern (steering vector) for $N_f$ antennas LIS deployment on (2), $\mathbf{y}$ the received signal from (1) and $\mathbf{y_f} \in \mathbb{C}^{M \times 1}$ the filtered output that represents the radio map. To guarantee the same output dimension (due to the 2D convolution along the LIS), we zero-pad $\mathbf{y}$ such that the output $\mathbf{y_f} \in \mathbb{C}^{M \times 1}$. To obtain a radio map, we just need to compute the energy at the output of the MF procedure $|\mathbf{y}_f| \in \mathbb{R}^{M \times 1}$. We then map the values to the RGB scale using the function $F : \mathbb{R}^{M \times 1} \rightarrow \{[0, 255] \cap \mathbb{N}\}^{M \times 3}$ such that $\mathbf{y}_m = F(|\mathbf{y}_f|)$. Fig. 2 shows an exemplary radio map. In the exemplary scenario, one active transmitter $U_a = 1$ is used, while three static scatterers are present in the environment. We see the three scatterers in the environment (the cylindric-like shapes) while we can also identify the highest peak representing the user transmission. The scatterers are captured because from the receiver LIS viewpoint, they act as virtual sources that are equivalent to LoS components, i.e., in (2) the different reflections are equivalent to a LoS path.

[1] The distance $z_u = 6.2$ is a parameter for the filter design. This does not imply that in the evaluation, all the transmitters or scatters are fixed at this distance. In our work, we set $f = 3.5$ GHz and $N = 4$ m.

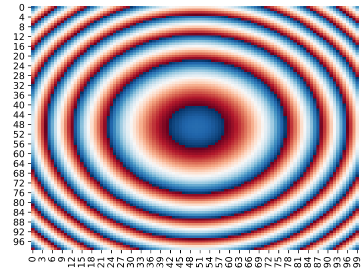

**Fig. 1**. Phase representation of the designed filter based on (2).

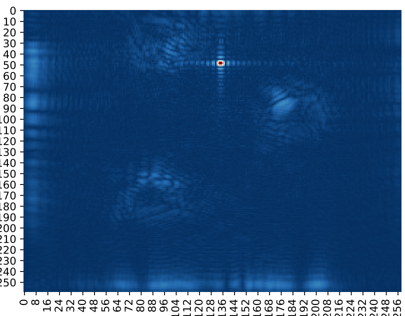

**Fig. 2**. Exemplary radio map obtained in a noiseless scenario with $U_a = 1$ users by using the MF design represented in Figure 1.

## 4. PASSIVE MULTI-HUMAN DETECTION BASED ON LIS RADIO MAP

### 4.1. Offline scanning phase

We first take advantage of an offline scanning period phase in which we measure different transmissions of any $U_a$ active devices to scan the static features of the propagation environment. We then obtain $U_a$ measurements of the environment for different random active user positions when no passive humans are in the scenario. Figure 2 shows that we have mainly two dominant ranges of pixel values, either low energy at the output of the MF (the background) or high energy (the active transmitter and scatterers). This leads us to apply a k-means clustering w.r.t. the pixel values of the radio map (with $k = 2$) to enhance the radio map through its binarization. We then define the clusterization as $K : \{[0, 255] \cap \mathbb{N}\}^{M \times 3} \rightarrow \{[0, 255] \cap \mathbb{N}\}^{M \times 1}$ such that $\mathbf{y}_c = K(\mathbf{y}_m)$. Figure 3a shows a clusterized version of the radio map presented in Figure 2. It shows the enhanced areas of the static features of the environment as well as the active transmitter. We use a computer vision technique called Template Matching [23], which detects parts in an image that matches a template image, to remove the expected active transmitter pattern from the clusterized map $\mathbf{y}_c$. By combining different active transmissions along the scenario, we can combine several radio maps to obtain an enhanced version that highlights the scatterers presence in the scenario, as shown in Figure 3b. These multiple transmission positions illuminate the scatterers from different angles. Furthermore, these map pixel values are either 0 (black) or 1 (white), being white the representation of the scatterers. We will denote this processed map as positive masking

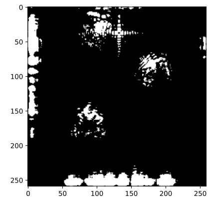

(a) Exemplary clusterized k-means map obtained by using the MF map in Figure 2.

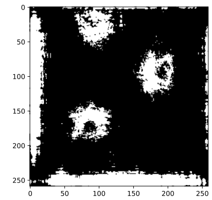

(b) Exemplary clusterized k-means positive masking map obtained by the combination of $U_a = 10$ random transmissions.

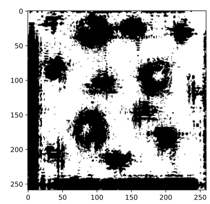

(c) Exemplary clusterized k-means negative masking map obtained by the combination of $U_a = 10$ random transmissions.

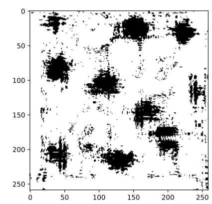

(d) Exemplary logical OR processed negative masking map obtained by the combination of $U_a = 10$ random transmissions.

**Fig. 3**. Radio map processing

map, $\mathbf{y}_{TM}^{+}$.

By having this representation of the static elements of the environment, we can now store $\mathbf{y}_{TM}^{+}$ locally at the LIS to process new maps and remove the static elements of it when trying to detect humans passively.

### 4.2. Detection phase

For this purpose, when there are passive humans in the room, we can follow the same procedure as before but obtaining a negative masking map $\mathbf{y}_{TM}^{-}$ (meaning scatterers are now black) for every temporal radio map snapshot $s \in S$. Figure 3c shows an example of a negative masking map $\mathbf{y}_{TM}^{-}$ when there is $U_p = 10$ passive humans in the scenario. We see now the scatterers and the humans are represented in black (0 value). Next, We will use it to perform a logical OR operation $(+)$ with the locally stored masking map $\mathbf{y}_{TM}^{+}$. Formally, we denote this operation as $\mathbf{y}_{OR} = \mathbf{y}_{TM}^{+} + \mathbf{y}_{TM}^{-}$. Furthermore, we obtain the OR map $\mathbf{y}_{OR}$, shown in Figure 3d, which eliminates the static scatterers of the scenario and highlights the passive humans reflections. We can see in the map that there are some artifacts (salt-pepper noise) as a result of this process. To alleviate it, we define a sliding window algorithm of size $K_c \times K_c$ that set all the pixel values comprising the window size to 1 (white) if the number of black pixels in that window is lower than a defined threshold $T_h$. In this way, we can reduce significantly this salt-pepper noise. Figure 4b shows the removal of the artifacts thanks to this procedure. Finally, we are interested in detecting these shapes associated to the passive human positions in the radio maps. For that, we adopt a computer vision algorithm named Component Labeling [24] which compares neighboring pixels to detect a shape that is assigned to the same label. Figure 4a shows the exemplary groundtruth scenario in which these maps are computed while Figure 4b shows the result of detecting the $U_p = 10$ passive humans. They

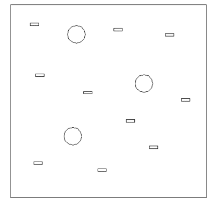

(a) Exemplary groundtruth scenario with $U_p = 10$ represented as rectangles.

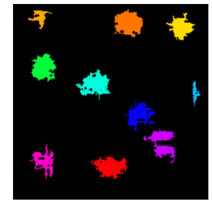

(b) Component Labeling applied to Figure 3d.

**Fig. 4**. Groundtruth position of the $U_p$ humans vs the Component Labeling result.

are assigned to different colors (labels) for illustration purposes. Hence, we can infer the passive human positions by obtaining the center pixel coordinates of these shapes $c_p = (x_p, y_p)$. To infer the real position, we just compute $c = c_p \times \Delta s$, where $\Delta s$ denotes the antenna spacing. Algorithm 1 further summarizes the procedure.

**Algorithm 1:** Passive multi-human localization

**Offline Scanning Phase:**
I. Measure the $U_a$ superposed complex baseband signal at the LIS, $\mathbf{y}$, as shown in (1)
II. $K$-means clustering with $K = 2$ is applied to the processed map $\mathbf{y}_m$ such that we obtain $\mathbf{y}_c$
III. Obtaining $\mathbf{y}_{TM}^{+}$ through Template Matching to eliminate the $U_a$ active transmitters
IV. Store locally $\mathbf{y}_{TM}^{+}$ at the LIS
**Detection phase:** Passive multi-human detection
**for** *each* $s \in S$ **do**
    I. Follow same procedure I-II from Offline Scanning Phase
    II. Obtaining $\mathbf{y}_{TM}^{-}$ through Template Matching to eliminate the $U_a$ active transmitters
    III. Computing the OR map $\mathbf{y}_{OR}$
    IV. Filtering salt-pepper noise with sliding window $K_c \times K_c$ and threshold $T_h$
    V. Applying Component labelling to detect the shapes of the $U_p$ passive humans
    VI. Compute $c$ to infer the locations
**end**

## 5. SIMULATION, NUMERICAL RESULTS AND DISCUSSION

### 5.1. Simulated scenario

We conducted simulations via ray tracing [25] to simulate the multipath in a reliable way. We simulate a scenario of size $10.34 \times 10.34 \times 8$ m. We deploy an LIS with $259 \times 259$ elements separated $\lambda/2$. Each $U_a$ active device transmits an arbitrary narrowband signal of 20 dBm at 3.5 GHz. The distance from which the MF is calibrated is $z_u = 6.2$. The active $U_a$ are assumed to be $\geq 1.8$ m height, being this value randomnly selected. The scatterers are modeled as metallic (with conductivity $s = 19444$ S/m, relative permittivity $\epsilon = 1$ and relative permeability $\mu = 20)^2$ cylinders of 1 m diameter and 2 m height. The passive $U_p$ humans are model as

[2] These values are provided by the software manual [25].

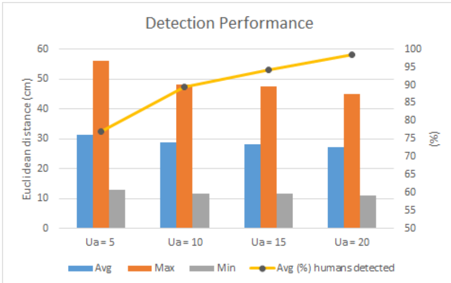


**Fig. 5**. Average human detection percentage (%) and positioning errors (cm) with fixed LIS aperture of $M = 259\times259$, in a $\gamma = 0$ dB condition, with $S = 100$ averaging strategy and $U_p = 10$ humans in the scenario.

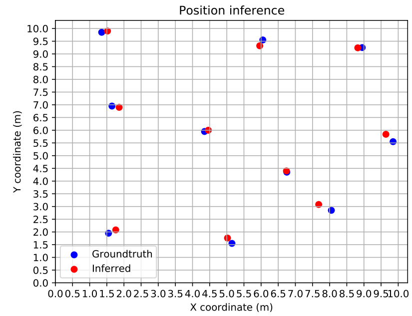


**Fig. 6**. Exemplary human detection with fixed LIS aperture of $M = 259 \times 259$, in a $\gamma = 0$ dB condition, with $S = 100$ averaging strategy, $U_a = 20$ active users and $U_p = 10$ humans in the scenario.

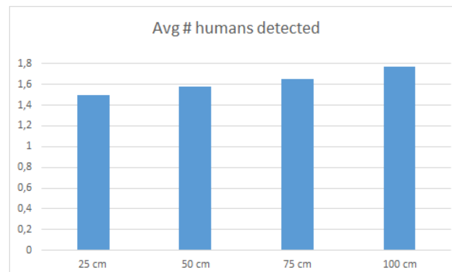


**Fig. 7**. Average human detection with fixed LIS aperture of $M = 259 \times 259$, in a $\gamma = 0$ dB condition, with $S = 100$ averaging strategy, $U_a = 20$ active users and $U_p = 2$ humans in the scenario.

rectangles of dimensions 0.3x0.5x1.7 m (average human dimensions obtained from [26]) with $s = 1.44$ S/m, $\epsilon = 38.1$ and $\mu = 1$ [27].

### 5.2. Received signal and noise modeling

From the ray-tracing simulation, the received signal in (1) is obtained as the complex electric field arriving at the $i$-th antenna element, $\widetilde{E}_i$, which can be regarded as the superposition of each ray path from every $u \in U_a$ user. Then, the complex signal at the output of the $i$-th element is therefore given by

$$y_i = \sqrt{\frac{\lambda^2 Z_i}{4\pi Z_0}}\widetilde{E}_i + n_i, \tag{4}$$

with $Z_0 = 120\pi$ the free space impedance and $Z_i$ the antenna impedance. For simplicity, we consider $Z_i = 1\,\forall\, i$. We define the average Signal-to-Noise Ratio (SNR), $\gamma$, is defined as

$$\gamma \triangleq \frac{\lambda^2}{4\pi Z_0 M\sigma^2}\sum_{i=1}^{M}|\widetilde{E}_i|^2. \tag{5}$$

We assume the system can obtain $S$ extra samples at each channel coherence interval to perform an S-averaging, diminishing the noise variance contribution.

### 5.3. Passive human detection

We here leverage the performance for passive human detection in the scenario using the method described in Section 4.1. We consider $U_p = 10$ humans at arbitrary positions in the scenario.

The detection of passive humans is highly impacted by the $U_a$ active devices positions. For the sake of generalization, we perform Monte Carlo simulations for obtaining our results under different random configurations. Figure 5 shows the average, maximum and minimum positioning errors of the correctly detected passive humans as well as the average detected humans by using a different number of active users $U_a$. Please note, we are not using dedicated active transmissions for this task, but we take advantage of the wireless communications occurring from these active devices in the scenario. The results show that the number of active users does not really impact on the positioning performance as it remains similar when using a lower and a higher number of active users $U_a$. However, by increasing $U_a$, the number of passive humans detected increases. This is because the more the transmissions, the more reflections we obtain from the human body reflections leading to an easier detection of the passive humans. Furthermore, the detection of this system is quite accurate, as we can detect a minimum of around 80% humans in all the configurations and the average error is around 28 cm. Figure 6 shows an illustration of the inferred positions w.r.t. the groundtruth positions. It shows the positioning accuracy is quite high even with 10 people passively sensed.

### 5.4. Passive human detection distance evaluation

Finally, we here evaluate the accuracy of the detection of passive humans by comparing performance under different separations among them. As we are interested in checking the distance at which the performance may decrease significantly, we set $U_p = 2$ humans separated 25/50/75/100 cm apart, respectively. We test different separations and we evaluate the detection performance of the $U_p = 2$ passive humans. Figure 7 shows the average detection of the humans. We can see the system achieves around 1.5/2 detections in the most challenging case (25 cm) while obtaining around 1.8/2 in the most favorable (100 cm). This shows the potential of the system, even when the separation among humans is quite small.

## 6. CONCLUSIONS

The presented use case shows machine learning and computer vision algorithms are a powerful tool to take into account when using an image-based LIS sensing approach. Moreover, we note that LIS is one of the technologies being considered for future 6G systems, which may change the relevant cost/benefit analysis in that any sensing functionality is then expected to be added onto the system rather than requiring explicit investment on extra dedicated hardware.

## 7. REFERENCES


[1] Cristian J Vaca-Rubio, Pablo Ramirez-Espinosa, Kimmo Kansanen, Zheng-Hua Tan, and Elisabeth de Carvalho, "Radio sensing with large intelligent surface for 6g," *arXiv preprint arXiv:2111.02783*, 2021.

[2] Fadel Adib, Zachary Kabelac, Hongzi Mao, Dina Katabi, and Robert C Miller, "Real-time breath monitoring using wireless signals," in *Proceedings of the 20th annual international conference on Mobile computing and networking*, 2014, pp. 261–262.

[3] Krzysztof Stasiak and Piotr Samczynski, "FMCW radar implemented in SDR architecture using a USRP device," in *2017 Signal Processing Symposium (SPSympo)*. IEEE, 2017, pp. 1–5.

[4] Joey Wilson and Neal Patwari, "Radio tomographic imaging with wireless networks," *IEEE Transactions on Mobile Computing*, vol. 9, no. 5, pp. 621–632, 2010.

[5] Donghoon Lee and Georgios B Giannakis, "A variational bayes approach to adaptive radio tomography," *arXiv preprint arXiv:1909.03892*, 2019.

[6] Grzegorz Kłosowski, Tomasz Rymarczyk, Przemysław Adamkiewicz, and Michał Styła, "The use of heterogeneous deep neural network system in radio tomography to detect people indoors," in *Proceedings of the 28th Annual International Conference on Mobile Computing And Networking*, 2022, pp. 859–861.

[7] Yongtao Ma, Wanru Ning, and Bobo Wang, "Training-free artifact detection method for radio tomographic imaging based device-free localization," *IEEE Transactions on Vehicular Technology*, vol. 70, no. 10, pp. 10382–10394, 2021.

[8] Mingmin Zhao, Tianhong Li, Mohammad Abu Alsheikh, Yonglong Tian, Hang Zhao, Antonio Torralba, and Dina Katabi, "Through-wall human pose estimation using radio signals," in *Proceedings of the IEEE Conference on Computer Vision and Pattern Recognition*, 2018, pp. 7356–7365.

[9] Mingmin Zhao, Yonglong Tian, Hang Zhao, Mohammad Abu Alsheikh, Tianhong Li, Rumen Hristov, Zachary Kabelac, Dina Katabi, and Antonio Torralba, "Rf-based 3d skeletons," in *Proceedings of the 2018 Conference of the ACM Special Interest Group on Data Communication*, 2018, pp. 267–281.

[10] Hao Wang, Daqing Zhang, Yasha Wang, Junyi Ma, Yuxiang Wang, and Shengjie Li, "RT-Fall: A real-time and contactless fall detection system with commodity WiFi devices," *IEEE Transactions on Mobile Computing*, vol. 16, no. 2, pp. 511–526, 2016.

[11] Qifan Pu, Sidhant Gupta, Shyamnath Gollakota, and Shwetak Patel, "Whole-home gesture recognition using wireless signals," in *Proceedings of the 19th annual international conference on Mobile computing & networking*, 2013, pp. 27–38.

[12] Youwei Zeng, Dan Wu, Jie Xiong, Jinyi Liu, Zhaopeng Liu, and Daqing Zhang, "Multisense: Enabling multi-person respiration sensing with commodity wifi," *Proceedings of the ACM on Interactive, Mobile, Wearable and Ubiquitous Technologies*, vol. 4, no. 3, pp. 1–29, 2020.

[13] Ying He, Yan Chen, Yang Hu, and Bing Zeng, "Wifi vision: Sensing, recognition, and detection with commodity mimo-ofdm wifi," *IEEE Internet of Things Journal*, vol. 7, no. 9, pp. 8296–8317, 2020.

[14] Xinbin Shen, Lingchao Guo, Zhaoming Lu, Xiangming Wen, and Zhihong He, "Wirim: Resolution improving mechanism for human sensing with commodity wi-fi," *IEEE Access*, vol. 7, pp. 168357–168370, 2019.

[15] Kai Niu, Xuanzhi Wang, Fusang Zhang, Rong Zheng, Zhiyun Yao, and Daqing Zhang, "Rethinking doppler effect for accurate velocity estimation with commodity wifi devices," *IEEE Journal on Selected Areas in Communications*, 2022.

[16] Bohan Yu, Yuxiang Wang, Kai Niu, Youwei Zeng, Tao Gu, Leye Wang, Cuntai Guan, and Daqing Zhang, "Wifi-sleep: sleep stage monitoring using commodity wi-fi devices," *IEEE internet of things journal*, vol. 8, no. 18, pp. 13900–13913, 2021.

[17] Erik G Larsson, Ove Edfors, Fredrik Tufvesson, and Thomas L Marzetta, "Massive MIMO for next generation wireless systems," *IEEE communications magazine*, vol. 52, no. 2, pp. 186–195, 2014.

[18] Emil Björnson, Erik G Larsson, and Mérouane Debbah, "Massive mimo for maximal spectral efficiency: How many users and pilots should be allocated?," *IEEE Transactions on Wireless Communications*, vol. 15, no. 2, pp. 1293–1308, 2015.

[19] Cristian J Vaca-Rubio, Pablo Ramirez-Espinosa, Kimmo Kansanen, Zheng-Hua Tan, Elisabeth De Carvalho, and Petar Popovski, "Assessing wireless sensing potential with large intelligent surfaces," *IEEE Open Journal of the Communications Society*, vol. 2, pp. 934–947, 2021.

[20] Cristian J Vaca-Rubio, Dariush Salami, Petar Popovski, Elisabeth de Carvalho, Zheng-Hua Tan, and Stephan Sigg, "User localization using rf sensing: A performance comparison between lis and mmwave radars," *arXiv preprint arXiv:2205.10321*, 2022.

[21] Cristian J Vaca-Rubio, Roberto Pereira, Xavier Mestre, David Gregoratti, Zheng-Hua Tan, Elisabeth de Carvalho, and Petar Popovski, "Floor map reconstruction through radio sensing and learning by a large intelligent surface," *arXiv preprint arXiv:2206.10750*, 2022.

[22] Zhou Zhou, Xiang Gao, Jun Fang, and Zhi Chen, "Spherical wave channel and analysis for large linear array in los conditions," in *2015 IEEE Globecom Workshops (GC Wkshps)*. IEEE, 2015, pp. 1–6.

[23] Roberto Brunelli, *Template matching techniques in computer vision: theory and practice*, John Wiley & Sons, 2009.

[24] Azriel Rosenfeld and John L Pfaltz, "Sequential operations in digital picture processing," *Journal of the ACM (JACM)*, vol. 13, no. 4, pp. 471–494, 1966.

[25] "Feko, altair engineering, inc," `https://www.altairhyperworks.com/feko`.

[26] P Potkány, Marek Debnár, Miloš Hitka, and Miloš Gejdoš, "Requirements for the internal layout of wooden house from the point of view of ergonomics changes," *Zeszyty Naukowe. Quality. Production. Improvement*, 2018.

[27] Peter S Hall, Yang Hao, Yuriy I Nechayev, Akram Alomainy, Costas C Constantinou, Clive Parini, Muhammad R Kamarudin, Tareq Z Salim, David TM Hee, Rostyslav Dubrovka, et al., "Antennas and propagation for on-body communication systems," *IEEE Antennas and Propagation Magazine*, vol. 49, no. 3, pp. 41–58, 2007.